J. Fluid Mech. (1982), *vol.* 117, *pp.* 403–423
Printed in Great Britain

Transport near a vertical ice surface melting in saline water: experiments at low salinities

By VAN P. CAREY

Department of Mechanical and Aerospace Engineering,
State University of New York at Buffalo, Amherst, NY 14260, U.S.A.

AND BENJAMIN GEBHART

Department of Mechanical Engineering and Applied Mechanics,
University of Pennsylvania, Philadelphia, PA 19104, U.S.A.

(Received 14 January 1981)

Time-exposure photographs of the buoyancy-driven flow adjacent to a submerged vertical ice surface melting in 10‰ saline water are presented for ambient water temperatures between 1 and 15 °C. For ambient temperatures greater than 1·9 °C, the thermal and saline components of the buoyancy force are at least partially opposed to each other. Since most past studies of ice melting in saline water have concentrated on oceanic salinities, little is known about the complicated flow behaviour which results from these opposed buoyancy effects at ambient water salinities between fresh water and oceanic salinities (35‰).

The results presented here provide new insight concerning the subtle mechanisms which arise in such flows. Photographs of the entire flow field document the many different and complicated flow configurations that arise. At 10‰, as the ambient temperature is increased from 1 to 15 °C, regimes of upward, bi-directional and split flow are observed. In the latter circumstance, the flow is laminar and bi-directional over part of the ice surface and turbulent over the rest of the surface. Bi-directional flow results from reversal of part of the upward wake above the top of the ice surface. Split flow appears to be a consequence of the transition to turbulence of either the inner or outer portion of the laminar bi-directional flow. Measured velocity profiles, surface heat-transfer rates and interface temperatures agree well with the analytical results reported in a previous study for conditions that result in conventional boundary-layer flow. These experimental results, together with those of previous studies, indicate the approximate extent of the different flow regimes that arise for a vertical ice surface melting in cold, low-salinity water.

1. Introduction

The buoyancy-driven flow near a vertical ice surface melting in cold pure or saline water has been the subject of a number of recent studies. Knowledge of such flows is important for understanding the transport behaviour near ice masses in terrestrial waters. The great preponderance of ambient conditions in the environment lie within the temperature and salinity ranges from −2 to 20 °C and 0 to 35‰. The experiments of Johnson (1978) and Josberger & Martin (1981) documented the complicated flow near a vertical ice slab melting in water at oceanic salinities, near 35‰. Carey &

Gebhart (1982) obtained similarity solutions for laminar natural convection flow adjacent to a submerged vertical ice surface melting in unstratified saline water. Numerical results were obtained for ambient temperatures t_∞ to 20 °C and ambient salinities s_∞ from 0 to 31‰. The complex flow near a vertical ice surface melting in cold pure water has also been investigated by Wilson & Vyas (1979); Gebhart & Mollendorf (1978); Carey, Gebhart & Mollendorf (1980) and Carey & Gebhart (1981). A detailed discussion of previous studies related to ice melting in saline water may be found in Carey & Gebhart (1982).

Here we present the results of an experimental investigation of the flow and transport near a vertical ice surface melting in saline water at intermediate salinities, between 0 and 35‰. The results presented here relate to ice-melting processes in coastal waters where sea water is locally diluted to low salinity by fresh water run-off. The purpose of the present study was two-fold. Experimental results are presented which test the accuracy of the similarity solutions of Carey & Gebhart (1982). In addition, experiments were conducted at $s_\infty = 10$‰ for the range of ambient temperatures where solutions were not obtained by Carey & Gebhart (1982). The observed flow behaviour is then combined with the results of the previous studies noted above to construct the first complete picture of the flow regimes that result for ambient conditions in the ranges $-2\ °C \leqslant t_\infty \leqslant 20\ °C$ and $0‰ \leqslant s_\infty \leqslant 35‰$. Specifically, a flow-visualization technique was used to examine the flow adjacent to a vertical ice surface melting in saline water, with $s_\infty = 10‰$ and $1\ °C \leqslant t_\infty \leqslant 15\ °C$. From photographs, local flow velocities have been determined and compared with the boundary-layer calculations of Carey & Gebhart (1982). Local heat-transfer data have also been inferred from the local ice-melting rates measured from the photographs. Thermocouples embedded in the ice were used to measure the interface condition $t_0(s_0)$ for each choice of ambient conditions t_∞ and s_∞. The results of these experiments provide a greater understanding of the mechanisms of these complicated flows.

2. Experiment

In this experiment, an ice slab 18·4 cm wide, 23·2 cm high and initially 3 cm thick was used. The ice was surrounded by 2·5 cm of expanded polystyrene insulation supported by an acrylic plastic 'picture frame' (see figure 1). To freeze the ice slab, the insulation and frame assembly was placed in a mould consisting of a shallow aluminium pan with plastic inserts to produce a protruding ice surface, 18 mm thicker than the plastic frame, with clean straight edges. The bottom of the mould was a 6 mm thick machined plate to ensure a flat ice surface. The mould was filled with de-ionized water that had been vigorously boiled to remove dissolved gases. The mould was then insulated on the top and sides and placed in a freezer where the water froze from the bottom upward. Any remaining dissolved gas thereby appeared as bubbles near the top of the ice.

After freezing, the mould was removed from the freezer and warmed to release the slab. The ice surface that formed at the bottom of the mould was bubble-free and had clean straight leading, trailing and side edges. When inserted into the tank, the flow along this surface was visualized. The back side of the ice slab, although less perfect, also melted during the experiment and provided symmetric wake conditions above and below the slab. Because the ice slab was moulded 18 mm thicker than the plastic

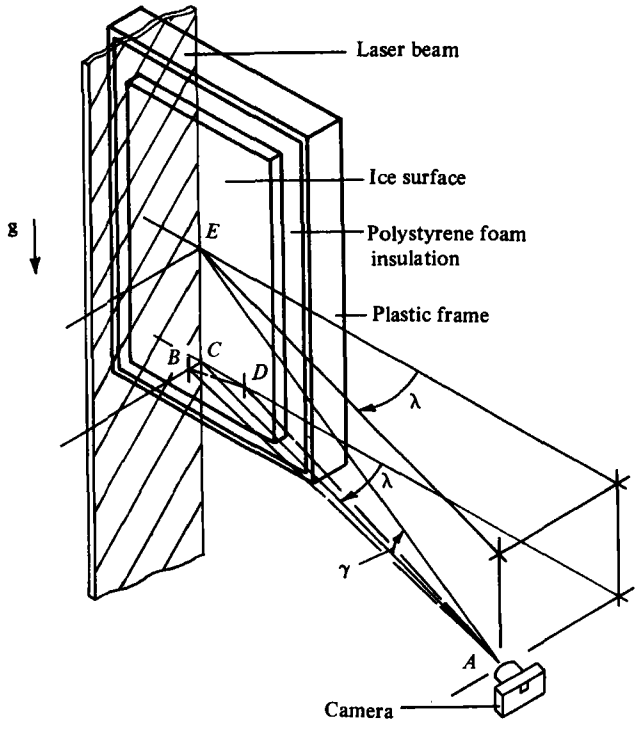

FIGURE 1. Schematic diagram showing the relative positions of the camera, ice surface and the laser beam.

fixture, when the slab was positioned vertically, the slab extended horizontally 9 mm out beyond the insulation and support frame on both sides (see figure 1). This provides horizontal leading and trailing edges and ensured that the flow near the leading and trailing edges was not strongly affected by the support frame.

After removing the slab from the mould, it was returned to the freezer and cooled below the interface temperature t_0 expected to occur during melting. Then the slab was removed from the freezer, placed in an insulating box and allowed to warm slowly to a temperature within 0·05 °C of the expected t_0. Two 0·013 cm diameter copper–constantan thermocouples were frozen into the ice slab. One was positioned near the midplane of the slab and the other near the surface. Both thermocouples were used to determine when the slab was equilibrated to the expected t_0. As the ice surface receded during the melting process, the bead of the thermocouple near the surface approached and passed through the interface. At the instant the bead was visually observed to penetrate the ice surface, the temperature was recorded. Equilibration of the slab to the expected t_0 prior to immersion assured that there was no heat conduction into the interior of the ice slab during the experiment. At low temperatures, the ice slabs were equilibrated to the values of t_0 predicted by the similarity solution of Carey & Gebhart (1982). These values of t_0, at lower t_∞, were extrapolated to obtain estimates of t_0 at higher ambient temperatures. If the measured t_0 differed from the initial slab temperature by more than 0·05 °C, the experiment was repeated with the ice equilibrated to the measured t_0. The experiment at each set of ambient conditions was

repeated until the measured t_0 agreed with the initial slab temperature to within $\pm 0{\cdot}05$ °C.

The slabs were melted in a glass tank 86 cm deep, 69 cm long and 66 cm wide. The tank was filled to a depth of 80 cm with 10‰ saline water. The ambient water was made to resemble 35‰ sea water diluted with pure water to a concentration of 10‰. The artificial 35‰ sea water was made according to a precise recipe from Lyman & Fleming (1940) as described in Carey (1981). The resulting solution was then diluted with de-ionized water to obtain a 10‰ solution. Johnson (1978) compared this 35‰ recipe with a standard sample of sea water from the Institute of Oceanographic Sciences in Wormley, England. Measured conductivities of the solutions indicated that the salinities agreed to within 0·2‰.

To visualize the flow, 1·25 g of Pliolite, ground to 40 μm size, was added to the water. Pliolite is a solid white resin manufactured by Goodyear Chemical Company, which is virtually insoluble in water and has a specific gravity of 1·026. The 40 μm particles remain suspended in water virtually indefinitely. The horizontal beam of a 5 mW helium–neon laser was reflected off a first-surface mirror downward through a cylindrical lens which spread the beam in one direction. The spread beam, now approximately 2 mm by 60 mm in cross-section, continued down into the tank. Side scatter of the columnated light off of the Pliolite particles made them visible.

The tank was surrounded by 7·6 cm of fibre-glass insulation which, for the lowest water temperature considered here, limited the bulk temperature rise of the water in the tank to less than 0·04 °C per hour. Prior to each experiment the salinity of the water was corrected to 10‰ by adding a small amount of concentrated solution of the recipe to the tank. The salinity was checked by comparing the electrical conductivity of the water in the tank with that of sea water made from the recipe. The electrical conductivity of the sea water was measured using a Beckman RC-19 conductivity bridge and dip cell. The accuracy of the system is rated at 0·25 % of reading, which corresponds to 0·2‰ at salinities near 35‰. At salinities near 10‰ the accuracy is slightly better. The exact salinity was determined by finding the ratio of conductivity of the tank water to that of the standard at the same temperature. Using this ratio and the ambient temperature, the salinity was calculated using the JPOTS tables (Joint Panel on Oceanographic Tables and Standards 1966). After adjusting the salinity to $10 \pm 0{\cdot}01$‰, the tank temperature was reduced to the desired level t_∞ using a circulating chiller. The tank water was stirred for 15 min after the chiller was removed to eliminate any non-uniformity in temperature. The tank was then allowed to stand for 40 min to let the viscous effects damp out the residual motion from the stirring.

After preparing the tank in this manner and equilibrating the ice slab to the expected t_0, the frame surrounding the ice slab was attached to a support fixture and the slab at the end of the assembly was lowered slowly into the tank. The support fixture was pre-adjusted such that when the slab was fully submerged, the ice surface was vertical to within $\pm 2°$ and the laser beam was aligned perpendicular to the ice surface. When a section of the insulation surrounding the tank was removed, the particles in the beam could be seen through the glass walls of the tank. The ice was allowed to melt for approximately 5 min after immersion to permit transient effects to die out. Time-exposure photographs of the flow were then taken using a motor-driven 35 mm Nikon camera, controlled by a Nikon intervalometer. The length of

the time exposure and the interval between photographs could be controlled by the intervalometer to an accuracy of $\pm 0{\cdot}05$ s. A running clock was started when the ice was immersed, and the time when each photograph was taken was recorded. This made it possible to compute the elapsed time between any two photographs taken while the ice slab melted.

The relative position of the ice slab, the light beam and the camera may be seen in figure 1. Of particular note in figure 1 is that the line of sight of the camera is at a small angle λ to the plane of the ice surface. The camera was positioned in this manner intentionally in order to determine the position of the ice surface in the photograph of the flow. To align the camera precisely along the ice surface would be difficult to do with great accuracy and would require continual adjustment since the ice surface recedes as it melts. At small λ, the viewer at point A in figure 1 will see the streak due to particle B directly and he will also see the reflected image of B at point D in the ice surface. For the small angles here, it is easily shown that the position of the ice surface in the plane of the beam, at point C in figure 1, can be determined to great accuracy by bisecting the angle BAD. This amounts to simply bisecting the distance in the photograph between the streak lines near the surface and their respective reflected images. Thus the position of the ice surface can be determined from the photographs without adjusting the camera position. The distance between the camera and the plane of the beam was recorded for each experiment and used to correct distances measured from the photographs from azimuthal (λ) and altitude (γ) angle effects. Photographs were taken for ambient water temperatures from 1 to 15 °C.

3. Results and discussion

Figures 2–7 show time-exposure photographs of the flows that result at ambient temperatures of 1, 2, 2·5, 5, 10 and 15 °C, respectively. In the left portion of each photograph are two reference wires 1·0 cm apart, indicating the scale of the flow. Figure 2, a 10 s time exposure for $t_\infty = 1$ °C, indicates that the flow is a fully upward, conventional boundary-layer flow. This is in agreement with the calculated results of Carey & Gebhart (1982), which found, at $(t_\infty, s_\infty) = (1, 10)$, that both buoyancy-force components were fully upward.

Figure 3 is a 10 s time exposure at $t_\infty = 2{\cdot}0$ °C. It can be seen that the flow near the surface is upward and boundary layer in character. However, there is now a weak downward flow outside. Photographs taken later in the experiment indicate that this outside downward flow is not a transient, but a steady-state feature. Because of the high Schmidt number, $Sc \simeq 2700$, and smaller Prandtl number, $Pr \simeq 12{\cdot}8$, the saline layer near the surface is much thinner than the thermal layer. The outer portion of the thermal layer is therefore entirely at the ambient salinity $s_\infty = 10$ ‰. For a salinity of 10 ‰, the density extremum occurs at $t_m(1, 10) = 1{\cdot}908$ °C. Thus, in the outermost portion of the thermal layer, where t is about the same as t_m, the fluid is more dense than the ambient at $t_\infty = 2$ °C. The buoyancy force there is then downward. Closer to the surface, where t is much less than t_m, the buoyancy force is upward.

Visual observations during the experiment indicated that the wake shed above the ice slab is the source of the outer downflow. The temperature of the fluid leaving the upper edge of the ice surface ranges between $t_0 = -0{\cdot}3$ °C and $t_\infty = 2$ °C. Recall that both sides of the ice slab are melting. The wakes from the two sides join above to form

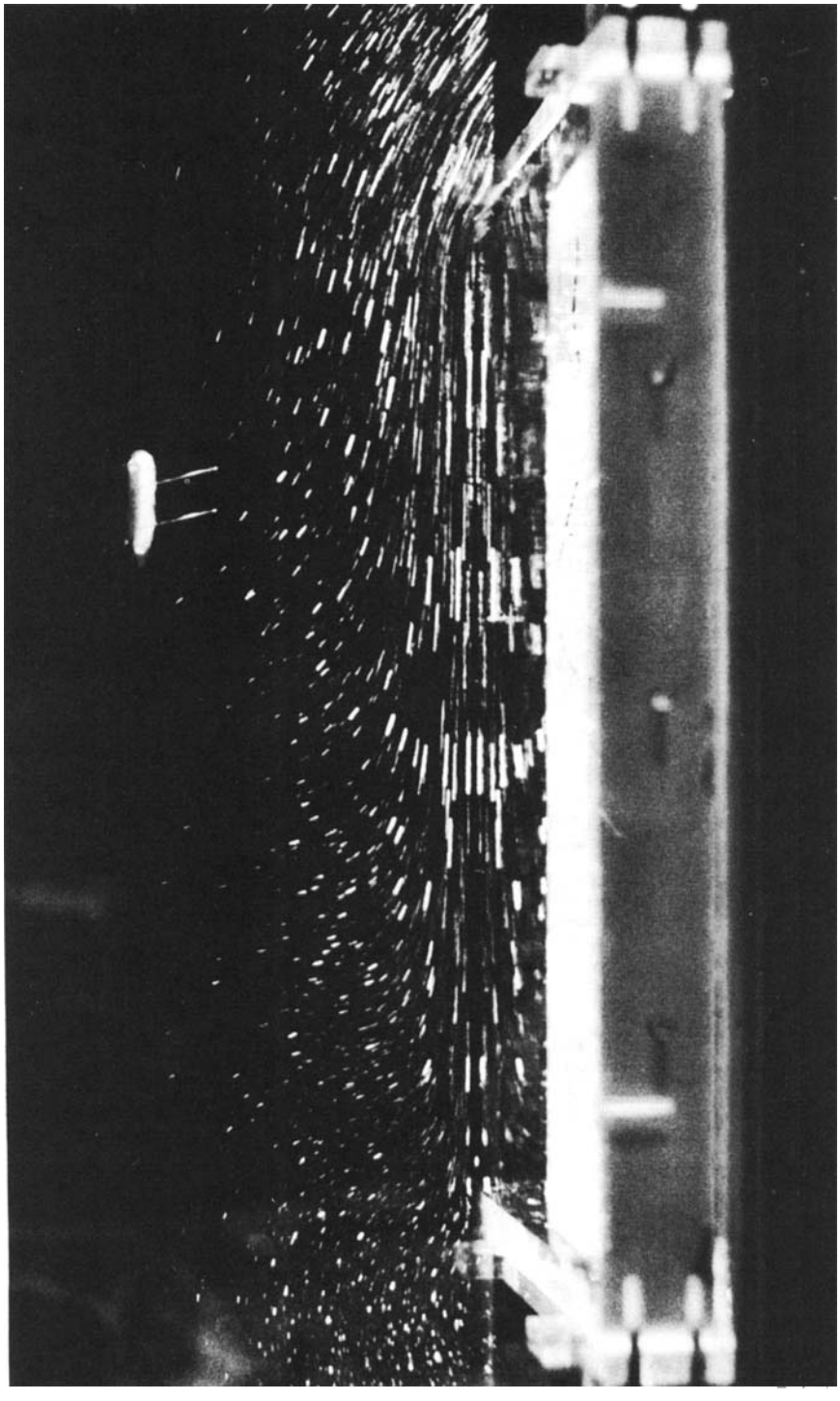

FIGURE 2. Flow adjacent to a vertical ice slab melting in saline water with $t_\infty = 1$ °C, $s_\infty = 10$ ‰. The length of the time exposure is 10 s. The reference wires are 1·0 cm apart.

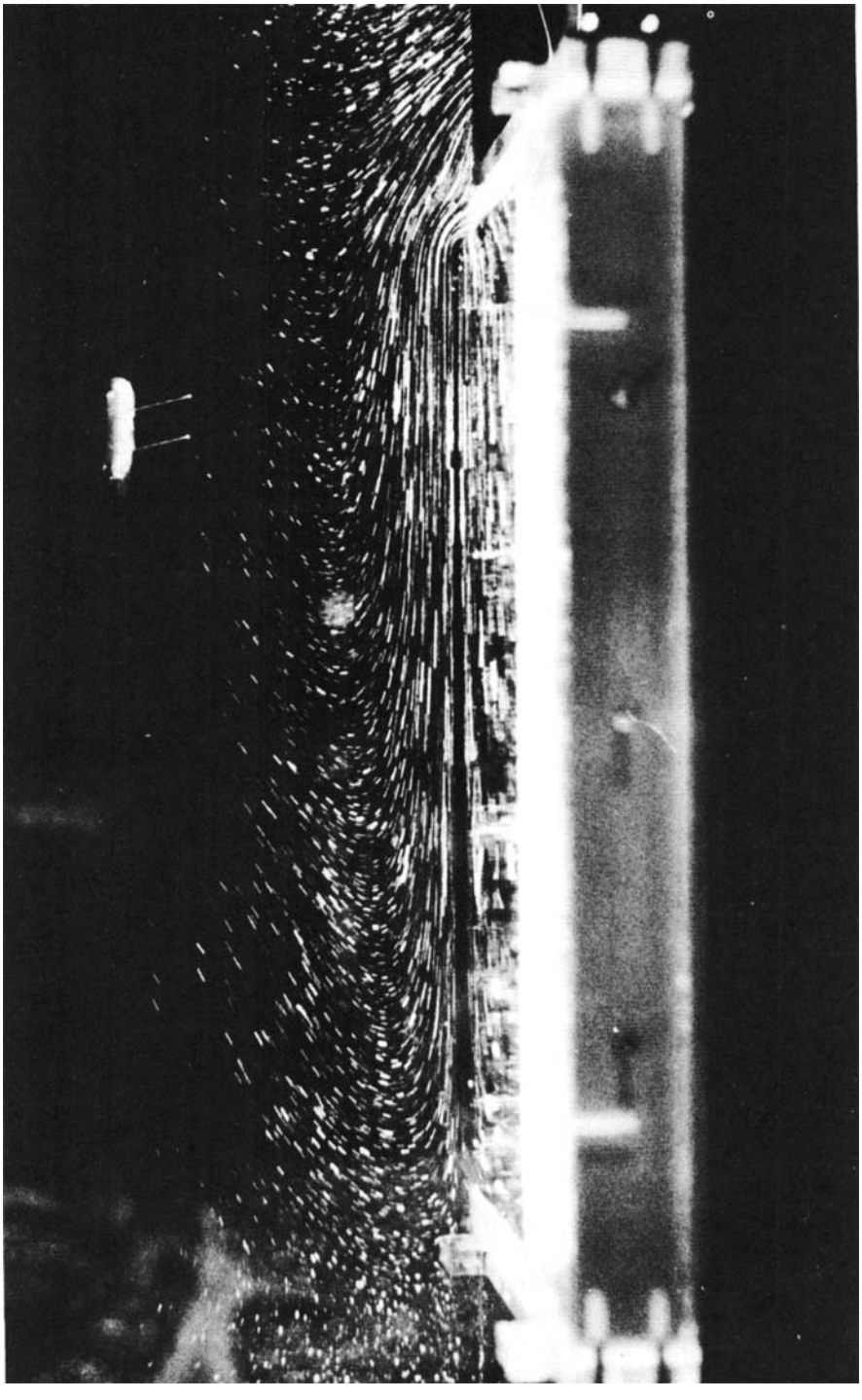

FIGURE 3. Flow adjacent to a vertical ice slab melting in saline water with $t_\infty = 2$ °C, $s_\infty = 10$ ‰. The length of the time exposure is 10 s. The reference wires are 1·0 cm apart.

a single buoyant jet. As fluid in the buoyant jet above the slab moves upward, it continues to entrain ambient fluid. Because the Lewis number is large, the thermal energy diffuses more rapidly into this jet than does the salt. The saline buoyancy remains confined to the centre of the jet. Near the outer edge of the jet, fluid at $s = s_\infty = 10\,‰$, warmed to near t_m, becomes more dense than the ambient. The resulting negative buoyancy there acts to decelerate and then recirculate some of this fluid downward. The other fluid in the wake travels upward until it reaches the air–water interface, 35 cm above the top edge of the slab. It forms a thin surface layer of cold, low-salinity water. Salinity diffuses more slowly than thermal energy. Therefore, near the top of this layer the fluid is both colder and less saline than the ambient. However, near the bottom of the layer, the fluid is colder with $s = s_\infty = 10\,‰$. Through conduction and mixing, some of the fluid in the lower portion of the layer warms to near t_m, whereupon it too begins to sink, eventually also feeding the weak downflow at the outer edge of the upward boundary layer near the surface. Thus the downflow arises from the warming of the fluid in the wake and, to a lesser degree, from warming of the cold fluid that collects at the air–water interface. Examination of photographs taken at different times during the experiment indicated that the outer downflow varies weakly with time. This is not surprising, since a laminar jet, like the one above the slab, is known to become unstable at small downstream distances.

The wake reversal, which complicates interpretation of the flow behaviour, is a consequence of fully immersing the ice slab in the water. The flow would be more complicated, however, if the slab were partially immersed, since the flow close to the ice surface would interact with the stratified surface layer described above. As long as the flow near the top of the ice surface is laminar, the mechanism for reversal will be present in the wake. However, if the flow at the top of the ice were turbulent, the strong upward saline buoyancy would dominate and no wake reversal would occur. This suggests that the wake reversal and outer downflow will occur for any finite ice slab whose length does not exceed the distance at which transition occurs.

At $t_\infty = 2{\cdot}5$ °C, figure 4, the flow near the surface also looks like boundary-layer flow. However, away from the surface, near its upper portion, a strong downflow exists. This, together with the upward flow, forms an almost cellular pattern on the upper half of the surface. Photographs taken at other times during the experiment again indicate some weak variation of the outer flow with time. However, the basic flow pattern remained unchanged during the experiment. The mechanism producing the outside downward flow is the same as that for $t_\infty = 2{\cdot}0$ °C, except that the downward buoyancy force for fluid in the wake, which warms to t_m, is stronger.

Note also the fluid moving horizontally in the light beam above the support fixture in figure 4. This fluid moves inward until it reaches the region just above the horizontal edge of the support fixture. There it turns upward and merges with the wakes from the front and back surfaces. The region near the top of the support fixture is not illuminated by the light beam in figure 4 so this turning cannot be seen. However, this behaviour was confirmed by visually observing the flow in that region during the experiment.

At $t_\infty = 5{\cdot}0$ °C, figure 5, the flow behaviour has changed completely from that observed at $t_\infty = 2{\cdot}5$ °C. The flow adjacent to the top of the ice surface is upward and turbulent. The flow over the lower portion of the surface is bi-directional and laminar.

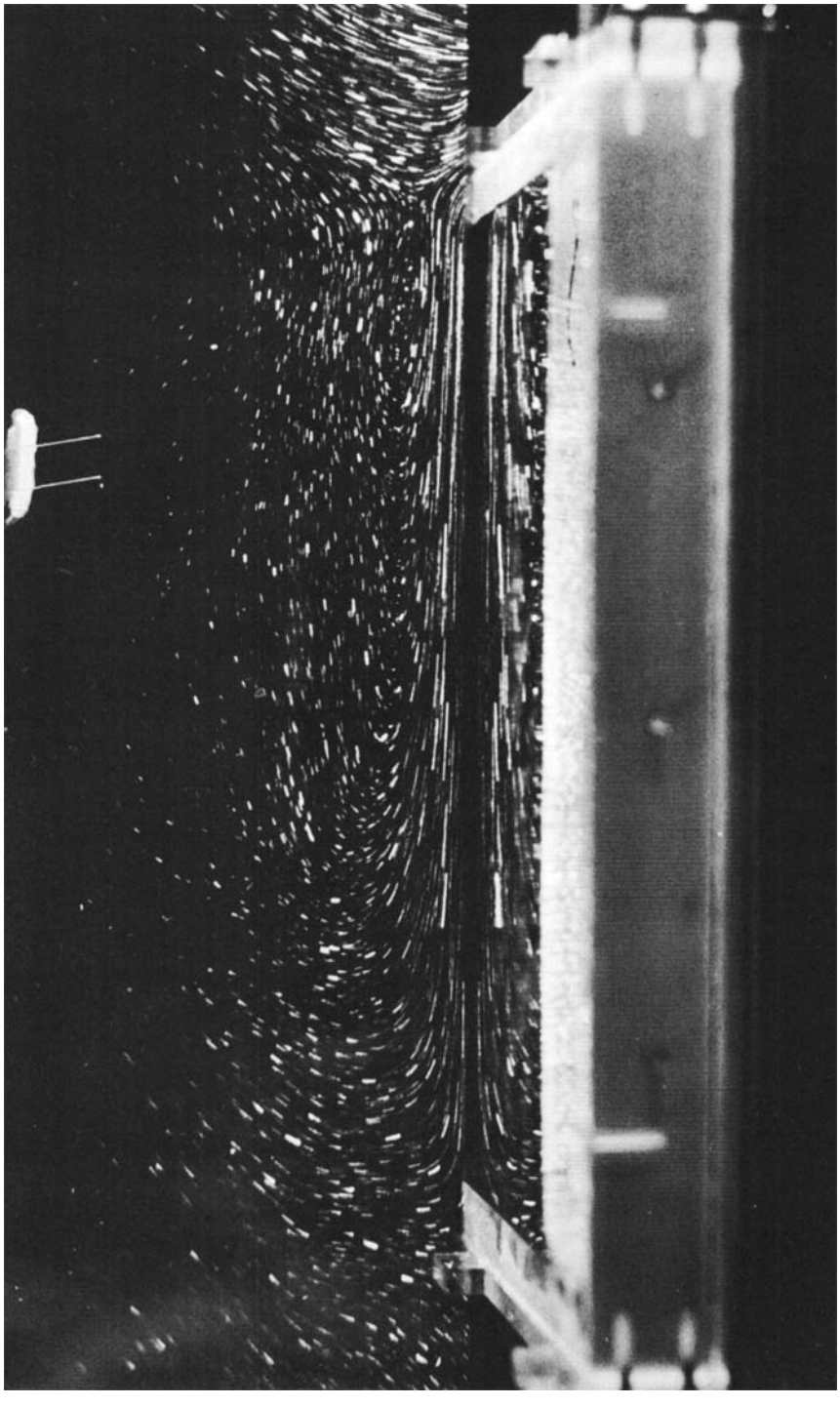

FIGURE 4. Flow adjacent to a vertical ice slab melting in saline water with $t_\infty = 2{\cdot}5\,^\circ\mathrm{C}$, $s_\infty = 10\,‰$. The length of the time exposure is 10 s. The reference wires are 1·0 cm apart.

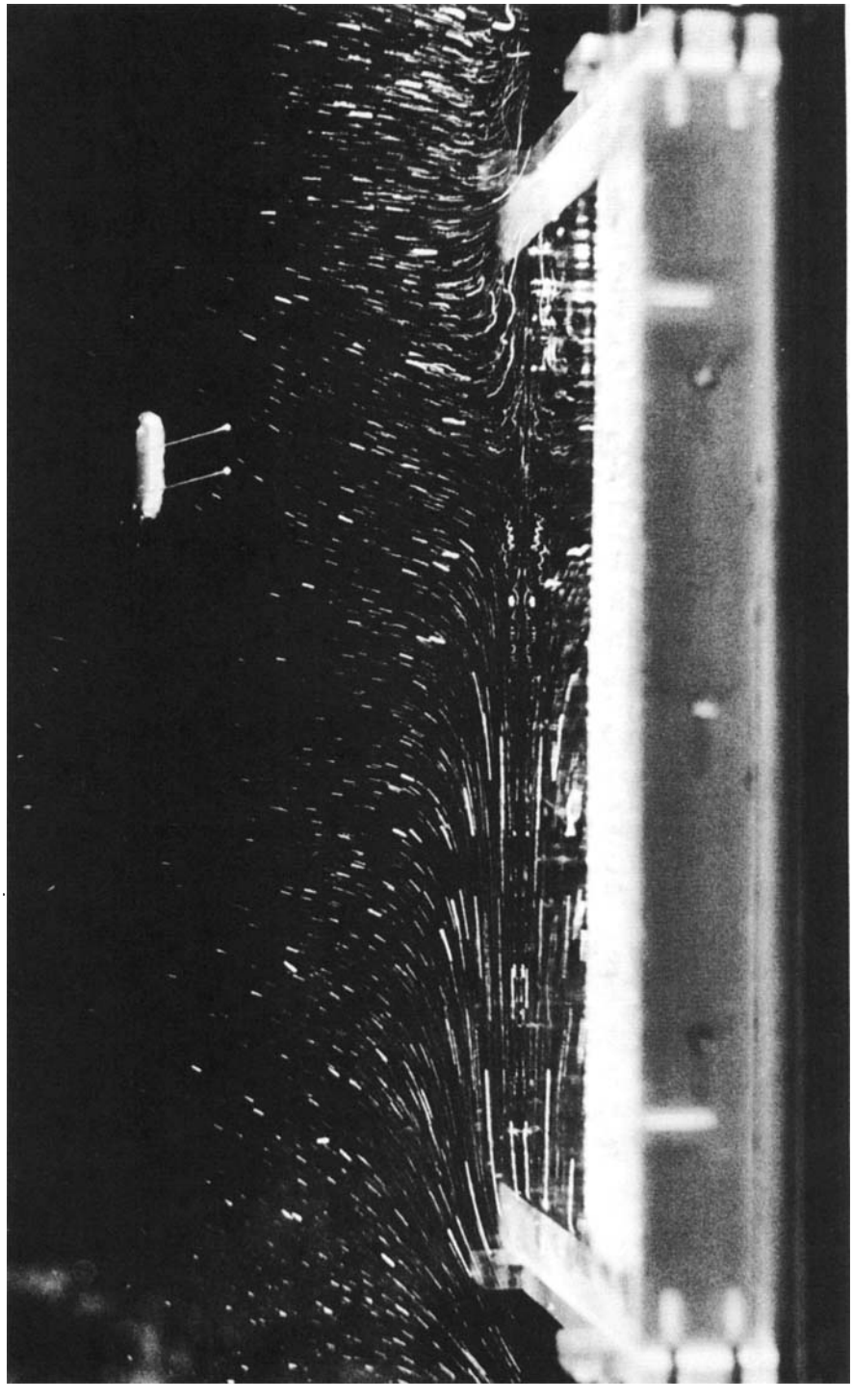

FIGURE 5. Flow adjacent to a vertical ice slab melting in saline water with $t_\infty = 5$ °C, $s_\infty = 10$ ‰. The length of the time exposure is 15 s. The reference wires are 1·0 cm apart.

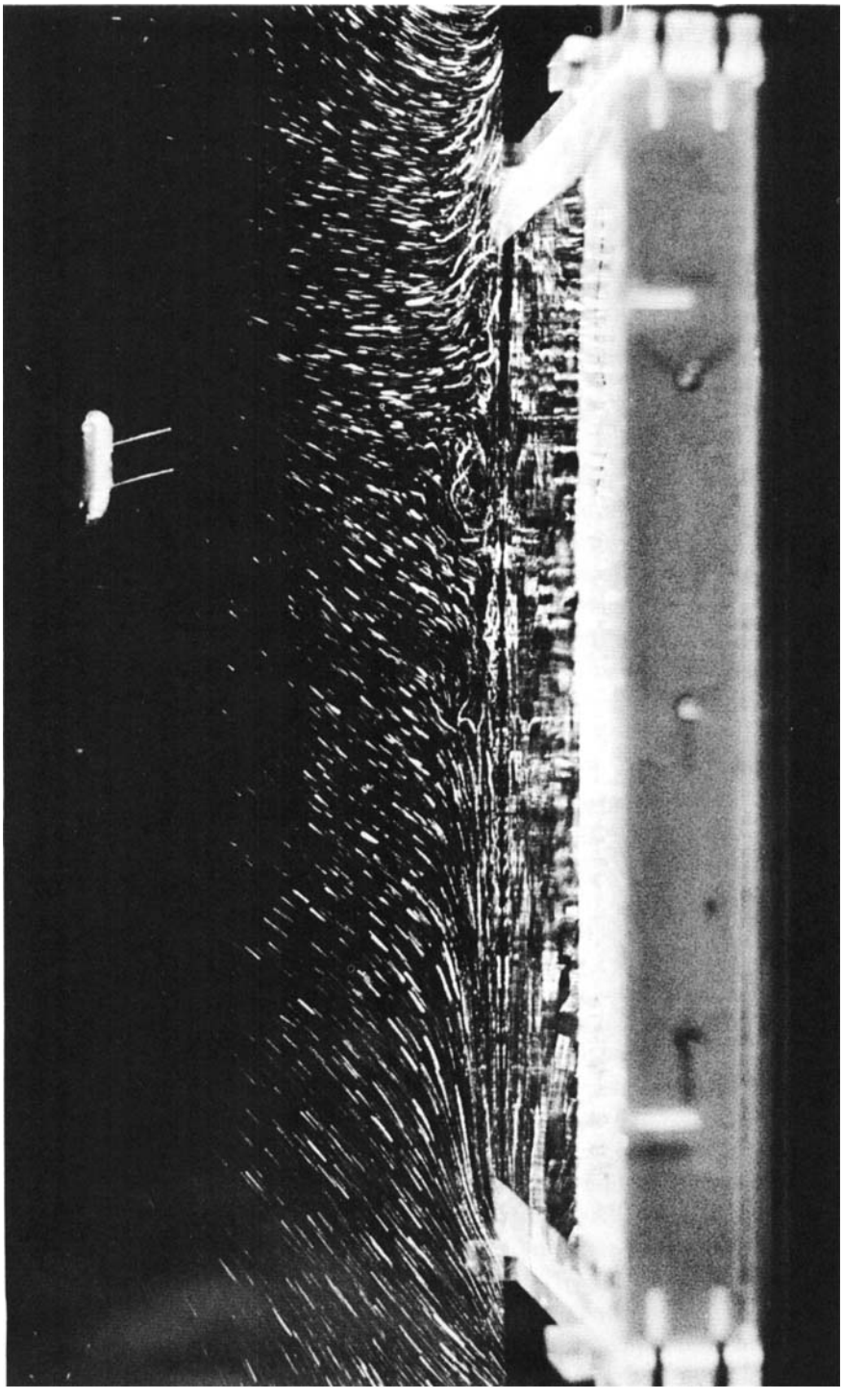

FIGURE 6. Flow adjacent to a vertical ice slab melting in saline water with $t_\infty = 10\,°C$, $s_\infty = 10\,‰$. The length of the time exposure is 10 s. The reference wires are 1·0 cm apart.

Let L be the height of the ice slab and x be the distance from the lower edge. A $x \simeq \frac{3}{4}L$, the entrainment from the ambient medium splits, with the upper portion feeding the upper turbulent flow and the lower portion feeding the lower laminar flow. Details of the turbulent flow cannot be determined fully from the photograph because the particles are visible only for the brief time they pass through the beam. However, the flow in the turbulent region is no longer two-dimensional. This photograph shows a projection in the plane of the beam of the particle's three-dimensional motion. The streaks for some particles appear helical, suggesting streamwise vorticity. After the ice had melted for approximately 30 min, the lower portion of the ice was still smooth. The upper portion, however, showed a number of vertical trough-like depressions, with a transverse wavelength of about 2·5 cm. This suggests a streamwise vortex motion, superimposed on the finer structure seen in figure 5. This motion locally enhances the heat transfer, producing the surface depressions.

Just above the halfway point on the surface, the flow is laminar and downward on the outside and turbulent and upward closer to the surface. However, further down, say for $x < \frac{1}{2}L$, the flow is laminar and bi-directional. Although it is difficult to see in figure 5, during the experiment a thin region of upward laminar flow was observed adjacent to the lower portion of the ice surface. Farther out, the flow is down. This implies that the upward saline buoyancy dominates in a thin region near the surface, whereas farther from the surface the flow is more strongly affected by the downward thermal buoyancy. Apparently the inner region, driven upward by the large saline buoyancy, becomes unstable and undergoes transition. The turbulence first appears near the surface, in figure 5, at $x \simeq \frac{1}{2}L$. The thickness of the turbulent region increases with downstream distance, that is, in the upward direction. At $x \simeq \frac{3}{4}L$, the turbulence apparently mixes the thermal and saline buoyancy together. The saline buoyancy thereby overcomes the effect of thermal buoyancy, resulting in fully upward turbulent boundary-layer flow.

At $t_\infty = 10$ °C, it can be seen in figure 6 that the flow behaviour is similar to that seen at $t_\infty = 5$ °C. Near the top of the surface, the flow is turbulent and upward. Very near the bottom edge of the ice, the flow is laminar and downward. The entrainment again splits, at $x \simeq \frac{3}{4}L$, with the upper portion feeding the upward flow and the lower portion feeding the downward flow. However, the flow does differ from that at 5 °C. At 5 °C the flow near the lower edge of the surface is bi-directional. However, at 10 °C no upward laminar flow can be seen on the inside, over the lower portion of the surface. The flow is fully downward.

Some turbulent fluid, shed from the upper flow, is convected downward, but none penetrates below $x \simeq \frac{1}{2}L$. The turbulence may decay, or, if it mixes with low-salinity melt water, it may reverse and move upward along the surface. The strong thermal buoyancy that results for $t_\infty = 10$ °C apparently overcomes the saline-buoyancy effect in the laminar portion of the flow. The flow there is fully downward. When turbulence mixes the saline and thermal buoyancy, the saline buoyancy again dominates, and the turbulent flow near the top of the surface is again upward.

After the surface had melted for about 20 min, the entire ice surface had a number of vertical trough-like depressions. These were similar to those observed only on the top portion of the ice surface at $t_\infty = 5$ °C. However, at $t_\infty = 10$ °C, these troughs covered virtually the entire surface. Their appearance over the entire surface further

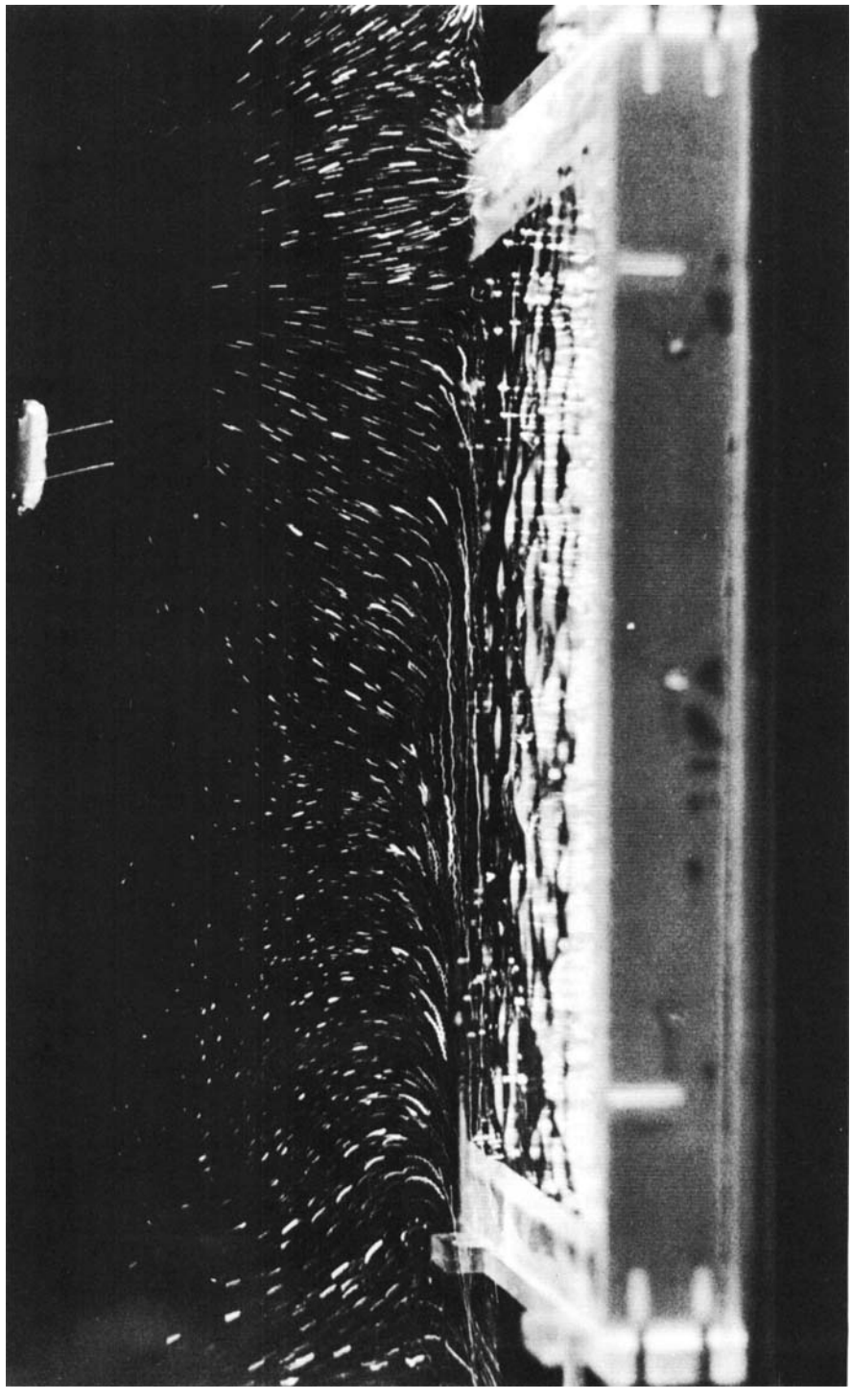

FIGURE 7. Flow adjacent to a vertical ice slab melting in saline water with $t_\infty = 15\,^\circ\mathrm{C}$, $s_\infty = 10\,‰$. The length of the time exposure is 10 s. The reference wires are 1.0 cm apart.

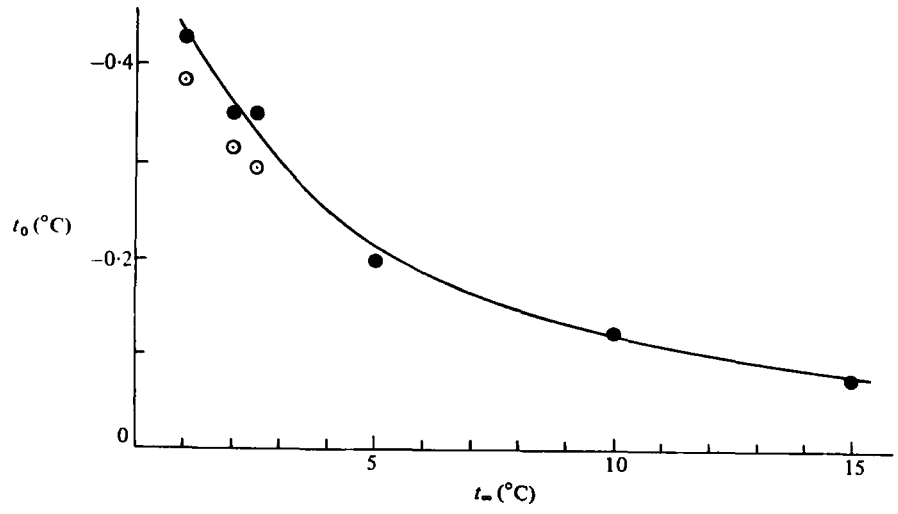

FIGURE 8. Measured interface temperatures (●) as a function of t_∞, $s_\infty = 10‰$. Also shown (⊙) are the computed values of Carey & Gebhart (1982) for low t_∞.

confirms the presence of turbulence near the surface at a lower location at $t_\infty = 10$ °C than at 5 °C.

As seen in figure 7, at $t_\infty = 15$ °C, the flow has changed completely from its behaviour at $t_\infty = 10$ °C. The entrainment appears to split very near the top of the ice surface. Over most of the surface, the flow appears to be downward and turbulent. The wavy particle streaks suggest either helical motion or sinusoidal motion. Although the ice surface is perfectly smooth and flat when immersed, the surface rapidly became very irregular, as seen by the mottling in figure 7. Strong variation in the local melt rate apparently results from large-scale turbulence in the flow. The portion of the ice surface above the location where the entrainment splits is so small that it is impossible to determine the nature of the flow there. The strong thermal buoyancy which results at this high ambient temperature apparently overcomes the saline buoyancy, producing downward turbulent flow over most of the ice surface.

In figure 8, the measured interface temperature is plotted as a function of ambient temperature for $s_\infty = 10‰$. The interface conditions at low temperature, calculated by Carey & Gebhart (1982), are also shown. The measured interface temperatures are also listed in table 1. At ambient temperatures less than 2·5 °C, the flow near the ice surface is laminar and upward. Josberger & Martin (1981) found that for $(t_\infty, s_\infty) = (0{\cdot}05, 14{\cdot}2)$ and $(1{\cdot}80, 8{\cdot}0)$ the flow was laminar and fully upward. Measurement of the surface temperature along the surface for these conditions indicated that t_0 and s_0 were essentially constant. The measurements in figure 8 were made by one thermocouple at a single vertical location, halfway up the surface. Based on the results of Josberger & Martin (1981), we expect that our measured value indicates the temperature of the entire surface for $t_\infty \leqslant 2{\cdot}5$ °C. For $t_\infty \geqslant 5$ °C the convective-transport mechanisms were observed to be non-uniform along the ice surface. Since the interface conditions are dictated by the local transport, the interface conditions will probably vary along the surface. Our measured value of t_0 halfway up the ice surface is therefore interpreted as a mean surface temperature. A consistent trend of increasing interface temperature with

t_∞ (°C)	Measured t_0 (°C)	Calculated t_0 (°C)	$\bar{x}$ (cm)	Measured $\dot{M}_{\bar{x}}$ (cm/day)	Calculated $\dot{M}_{\bar{x}}$ (cm/day)
1	−0·44	−0·38	17·2	4·32	3·96
2	−0·36	−0·31	19·1	6·63	6·67
2·5	−0·33	−0·29	15·1	7·42	8·10
5	−0·21				
10	−0·09				
15	−0·08				

TABLE 1. The measured surface temperature t_0 for each of the experimental conditions, and, for $t_\infty \leqslant 2{\cdot}5$ °C, the measured local melt rate $\dot{M}_{\bar{x}}$ at vertical location $\bar{x}$ on the ice surface. Also shown, for $t_\infty \leqslant 2{\cdot}5$ °C, are the corresponding local melt rate and interface temperature computed by Carey & Gebhart (1982). All results are for $s_\infty = 10\,‰$.

increasing t_∞ is observed. At low ambient temperatures, the measured surface temperature is seen to agree well with those predicted by the calculations of Carey & Gebhart (1982).

In addition to showing the general flow features, the photographs provide quantitative information about both the flow velocities and the local heat transfer rates. To determine the velocity at various points in the flow, the projected lengths of particle streaks parallel to the ice surface were measured from an enlarged time-exposure photograph of the flow field. The velocity parallel to the ice surface was computed by dividing the measured length by the length of the time exposure and correcting for the small-angle optical effects discussed in § 2. Likewise, the distances from the centre of the streak to the leading edge and to the ice surface were measured and corrected for small-angle effects. The streak lengths and positions were measured to an accuracy of $\pm 0{\cdot}25$ mm. The measured velocities were thereby accurate to within $\pm 2\,\%$ of the maximum velocity in the flow. The velocity and position measurements were then converted to the similarity variables of Carey & Gebhart (1982) with the following relations:

$$f' = \frac{u\bar{x}}{2\nu(Gr_{\bar{x}})^{\frac{1}{4}}}, \quad \eta = \frac{\bar{y}}{\bar{x}}(\tfrac{1}{4}Gr_{\bar{x}})^{\frac{1}{4}}, \tag{1), (2}$$

$$Gr_{\bar{x}} = \frac{\rho_m(0,1)}{\rho_m(s_\infty,1)}\frac{gg_{10}\bar{x}^3(s_\infty - s_0)}{\nu^2}. \tag{3}$$

Here $\bar{x}$ and $\bar{y}$ are the instantaneous downstream and surface-normal co-ordinates and u is the velocity parallel to the surface. The constants g and ν are the gravitational acceleration and kinematic viscosity, respectively, and $Gr_{\bar{x}}$ is the Grashof number. The values of $\rho_m(0,1)/\rho_m(s_\infty,1)$ and g_{10} are determined from the density correlation of Gebhart & Mollendorf (1977) as

$$\rho_m(0,1)/\rho_m(s_\infty,1) = 1/[1+g_{10}s_\infty], \tag{4}$$

$$g_{10} = 8{\cdot}046\,157 \times 10^{-4}. \tag{5}$$

The resulting data for flows at $t_\infty = 1$, 2 and 2·5 °C are plotted in figure 9. Also shown in figure 9, as the curves, are the computed results of Carey & Gebhart (1982) for $t_\infty = 1$, 2 and 2·5 °C. At 1 °C the measured velocities are in excellent agreement with the theoretical predictions over the entire flow region. At $t_\infty = 2$ °C, the agree-

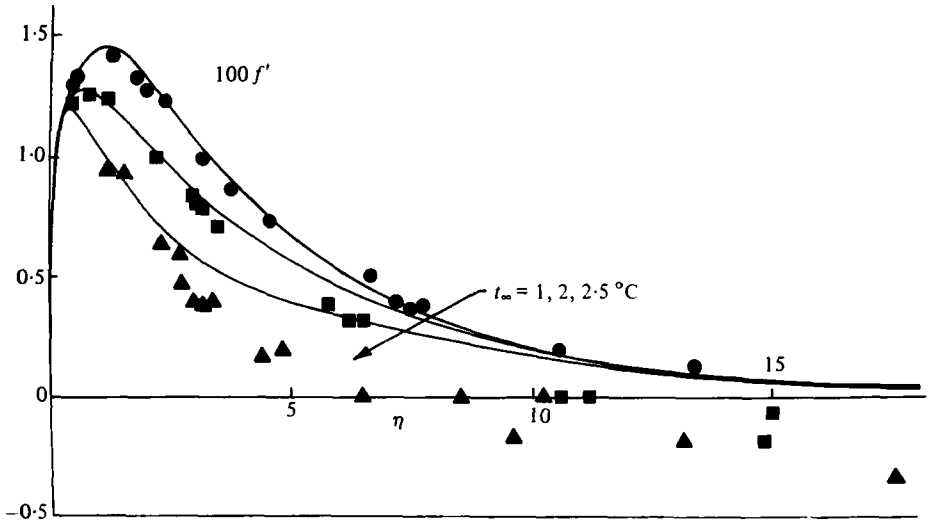

FIGURE 9. Measured velocity profiles for s_∞ = 10‰ and t_∞ = 1 °C (●), 2 °C (■) and 2·5 °C (▲). Also shown (——) are the computed profiles of Carey & Gebhart (1982).

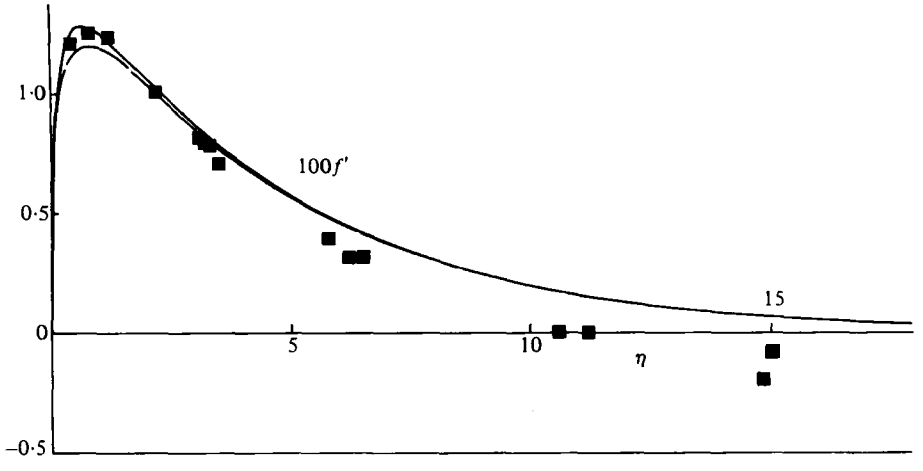

FIGURE 10. Measured velocity profile for s_∞ = 10‰ and t_∞ = 2 °C (■). Also shown are the profiles predicted by the analysis of Carey & Gebhart (1982) with (——) and without (— — —) interface-motion effects.

ment is good over most of the profile. However, at about $\eta = 5$ the experimental data points deviate, and at large η become slightly negative, indicating the outer downflow observed in the photographs. Similarly, at t_∞ = 2·5 °C the data agrees well with the theory near the surface, but the experimental results are much lower at larger η. At large η the measured velocities become negative. The downflow at large η for these conditions is a consequence of the wake reversing direction, moving downward and interacting with the upward flow near the surface. The theoretical formulation is based on a semi-infinite plate and therefore could never predict this outer downflow. Since the Schmidt number *Sc* and Prandtl number *Pr* are large, the thermal- and salinity-transport regions are close to the surface and therefore mostly in the region

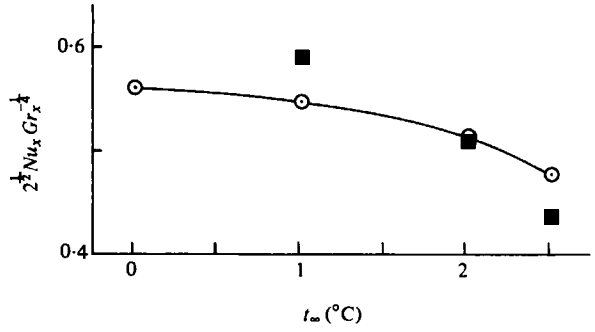

FIGURE 11. Measured local surface heat transfer (■) as a function of t_∞ at $s_\infty = 10‰$. Also shown (⊙) are the calculated values of Carey & Gebhart (1982).

where theory and experiment agree. This suggests that the interface conditions and surface heat transfer predicted by the theory may be accurate despite the fact that the predicted velocity is totally unrepresentative at large η.

Figure 10 again shows the measured velocity data for $t_\infty = 2{\cdot}0$ °C compared with the corresponding calculated velocity profile. The solution of Carey & Gebhart (1982) includes the effect of interface motion. Also shown in figure 10 is the computed velocity profile obtained if the motion of the interface is neglected. This was also computed using the analysis and the computational technique of Carey & Gebhart (1982). However, the normal velocity at the ice surface was taken as zero. This, in effect, neglects interface motion. It can be seen that the computed profiles differ significantly only near the maximum velocity. There, the measured data is seen to agree more closely with the velocity profile calculated with interface motion. It appears, therefore, that including the effect of interface motion is more accurate, even at relatively low ambient temperatures.

The photographs of the flow field were also used to compute the local heat transfer. In two photographs of the flow, taken at different times during the experiment, the position of the ice–water interface was determined by bisecting the streak pairs. In each of the two photographs, the distance from the end of the lower reference wire (in the left of each photograph) to the ice–water interface was measured along a line normal to the interface. The difference in the measured distances yields the melting rate during the time between photographs. Using the latent heat for ice to calculate the heat transfer, the following relation is obtained which relates the local Nusselt number to the measured quantities.

$$Nu_{\bar{x}} Gr_{\bar{x}}^{-\frac{1}{4}} = \frac{h_{\bar{x}} \bar{x}}{k} Gr_{\bar{x}}^{-\frac{1}{4}} = \frac{\bar{x}}{k Gr_{\bar{x}}^{\frac{1}{4}}} \frac{\Delta l}{\Delta \tau} \frac{\rho_1 h_{11}}{t_\infty - t_0}. \tag{6}$$

Here $h_{\bar{x}}$ is the local heat-transfer coefficient, k is the thermal conductivity of water, ρ_1 is the density of ice, h_{11} is the specific heat of fusion of ice, and Δl and $\Delta \tau$ are the measured changes in distance and time, respectively, between the photographs. The resulting data points are shown in figure 11, along with the predicted theoretical results of Carey & Gebhart (1982). The melt-rate data is also listed in table 1. Because the interface moves only a small distance in the time intervals considered here, the accuracy of the heat-transfer data is limited by the accuracy of the distance measurement to only about ± 15 %. Nevertheless, the measurements shown in figure 11 agree

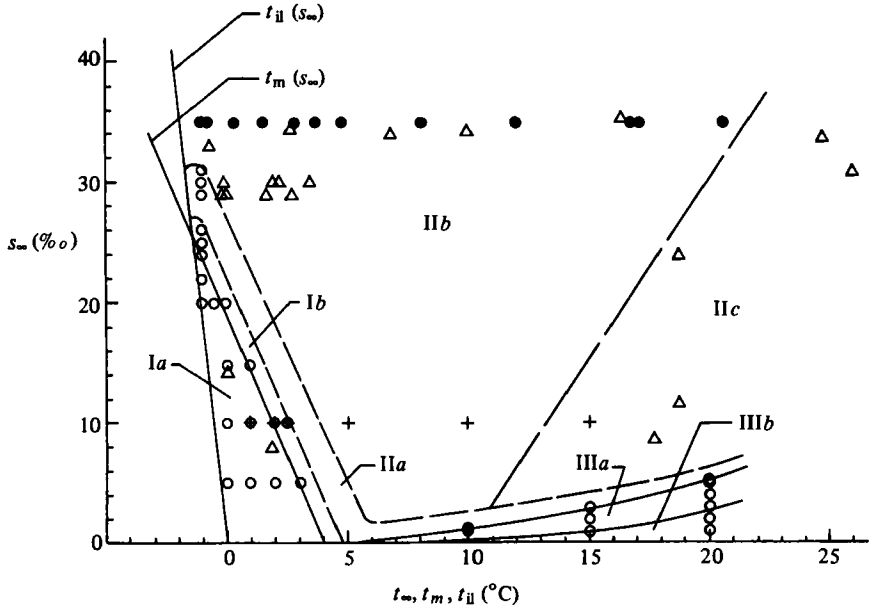

FIGURE 12. Flow regimes corresponding to different choices of t_∞ and s_∞ for flow adjacent to a vertical ice surface melting in saline water. Also shown are the points corresponding to the calculations of Carey & Gebhart (1982) (○), and the experiments of Johnson (1978) (●), Josberger & Martin (1981) (△), and those of the present study (+).

well with the calculated results. For $t_\infty = 2$ and 2·5 °C, as discussed above for the velocity measurements, the measured heat transfer agrees with the values predicted by the theory, despite the differences in the velocity profiles seen in figure 9.

4. Conclusions

The time-exposure photographs presented here document the nature of the natural convection flow adjacent to a vertical ice surface melting in 10‰ saline water at ambient temperatures from 1 to 15 °C. At $t_\infty = 1$ °C, the flow is laminar and fully upward. At this ambient temperature, the velocity profile measured from the time exposure photographs agrees well with the theoretical results of Carey & Gebhart (1982) all across the boundary layer. At $t_\infty = 2$ and 2·5 °C, laminar bi-directional flow results. At these temperatures, the experimental and theoretical velocity profiles agree near the ice surface. Farther from the surface, reversal of portions of the upward wake caused the measured velocity profile to deviate from the theoretical results for a semi-infinite surface. In spite of the wake reversal at $t_\infty = 2$ and 2·5 °C, the measured interface temperatures and surface heat transfer were found to be in good agreement with those predicted by Carey & Gebhart (1982) for $t_\infty = 1$, 2 and 2·5 °C. For $t_\infty = 5$ and 10 °C, split flow was found, with upward turbulent flow near the upper portion of the surface, and laminar downward or bi-directional flow near the lower portion. At 15 °C, the flow was downward and turbulent over most of the surface, with a small region of upward flow near the top.

From the results presented here and the results of Carey & Gebhart (1981, 1982), Johnson (1978) and Josberger & Martin (1981), it is possible to surmise the approxi-

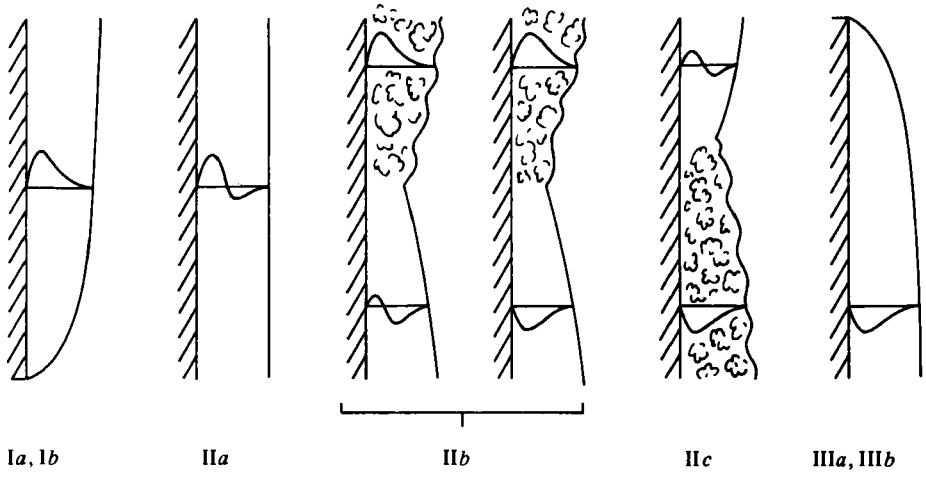

FIGURE 13. Flow patterns corresponding to the regions of the (t_∞, s_∞)-plane shown in figure 12.

mate extent of the different flow regimes that arise near a melting ice surface at ambient conditions in the ranges $-2\ °C < t_\infty < 20\ °C$ and $0 \leqslant s_\infty < 35‰$. Figure 12 shows the regions of the (t_∞, s_∞)-plane that correspond to different flow regimes, as indicated by the present results and those of previous studies. Also shown in figure 12 are the points at which Carey & Gebhart (1982) have calculated solutions, and the points at which experiments have been conducted in the present study and in studies by Johnson (1978) and Josberger & Martin (1981). The flow behaviour that corresponds to each regime is shown in figure 13. Similarity solutions were obtained by Carey & Gebhart (1982) in regions I*a*, I*b*, III*a* and III*b*. In regions I*a* and I*b*, the analytical results indicate fully upward flow. Our experiments indicate upward flow in I*a*, but bi-directional flow in I*b* due to reversal of part of the upward wake above the slab. In regions III*a* and III*b*, the computations of Carey & Gebhart (1982) indicate fully downward boundary-layer flow. The asymptotic calculations of Carey & Gebhart (1982), the experiments of Carey & Gebhart (1981) and some of the full calculations of Carey & Gebhart (1982), at high t_∞, all indicate that for the extensive range of conditions in region II*a*, laminar bi-directional flow results.

Josberger & Martin (1981) found that at salinities near 35‰ and $t_\infty < 18\ °C$, split flow resulted. For these conditions, the flow near the bottom portion of the surface was laminar and bi-directional. Over the top portion there was fully upward turbulent flow. These results at oceanic salinities, together with the present results indicate that split flow of this type occurs throughout region II*b* in figure 12. Two forms of this split flow arise in region II*b*. The first is that found by Josberger & Martin (1981), for which the laminar portion is bi-directional. The second form is that found here at $t_\infty = 10\ °C$, $s_\infty = 10‰$, for which the laminar portion is fully downward. It seems likely that this second form is more common at low salinity and high temperature, where the downward thermal buoyancy is larger relative to the saline buoyancy.

Johnson (1978) observed 'net upward' flow for $-0{\cdot}7 \leqslant t_\infty \leqslant 20{\cdot}7\ °C$. His schlieren photographs indicate a laminar region near the lower edge of the ice surface, with an upward turbulent region near the top. Although his results do not indicate whether the laminar region is bi-directional, his observations are in agreement with those

reported by Josberger & Martin (1981) for conditions in region II*b*. Johnson (1978) also reports melt-rate measurements for $t_\infty > 20{\cdot}7$ °C at 35‰, but for these conditions he did not investigate the flow behaviour. These high-temperature points, which lie in region II*b*, were not included in figure 12, since they provide no information about the flow near the surface.

For $t_\infty > 23$ °C, at oceanic salinities, Josberger & Martin (1981) found a split flow that is different from that found in region II*b*. For these conditions, near the lower portion of the slab he found fully downward turbulent flow, while near the top of the slab he found laminar bi-directional flow. For experiments at ambient salinities of about 24, 12 and 9‰ in region II*c*, he reports the same split-flow behaviour. His results, together with the present ones, indicate that this 'inverted' split flow occurs throughout region II*c*. It was not possible to determine the nature of the flow near the upper edge of the ice slab at $t_\infty = 15$ °C, $s_\infty = 10$‰ from our photographs. However, since the split flow is similar in character to that observed by Josberger & Martin (1981) for $t_\infty > 23$ °C at oceanic salinities, and at lower salinities in region II*c*, it seems likely that the flow near the top edge at $(t_\infty, s_\infty) = (15, 10)$ may also be laminar and bi-directional in character.

Regions I*b* and II*a* are apparently a transition between the simple boundary-layer flow in regions I*a* and III*a*, and the split-flow behaviour in regions II*b* and II*c*. The role of the length L of the slab as a parameter in these flows is not clear. The slab used for these experiments was smaller than that used by Josberger & Martin (1981), yet the flow behaviour is similar in many respects, suggesting that the slab length does not have a strong effect on such flows. Because the thermal- and saline-buoyancy forces are opposed, and $Le = Sc/Pr$ is large, the buoyancy force will be bi-directional for laminar flows in region II. Such flows will have very strong buoyancy-force and velocity gradients, which suggests that they may be very unstable. Hence it is not surprising that turbulent flow is found near the ice surface for conditions in region II*b* that are only slightly beyond the boundaries of regions I and III (see figure 12).

Figures 12 and 13 indicate the approximate extent of the different regimes of flow behaviour that occur for the ranges of t_∞ and s_∞ of usual interest in terrestrial waters. The location of the boundaries of some regions is not known exactly since the data is somewhat limited. Nevertheless, the general picture is now clear. It is apparent that for a wide range of ambient conditions of interest, non-boundary-layer flow results, with the flow being either bi-directional or of the split-flow type. Carey & Gebhart (1982) have analysed the boundary-layer circumstances. However, successful analysis of the non-boundary-layer flows will require a bit more ingenuity, owing to their very complicated nature.

The first author wishes to acknowledge graduate-fellowship support from the Graduate School at the State University of New York at Buffalo. The authors also wish to acknowledge support for this study by the National Science Foundation under research grants ENG77-21641 and DPP80-09250.

REFERENCES

CAREY, V. P. 1981 Transport in vertical mixed convection flows and natural convection flows in cold water. Ph.D. thesis, State University of New York at Buffalo.

CAREY, V. P. & GEBHART, B. 1981 Visualization of the flow adjacent to a vertical ice surface melting in cold pure water. *J. Fluid Mech.* **107**, 37–55.

CAREY, V. P. & GEBHART, B. 1982 Transport near a vertical ice surface melting in saline water: some numerical calculations. *J. Fluid Mech.* **117**, 379–402.

CAREY, V. P., GEBHART, B. & MOLLENDORF, J. C. 1980 Buoyancy force reversals in vertical natural convection flows in cold water. *J. Fluid Mech.* **97**, 279–297.

GEBHART, B. & MOLLENDORF, J. C. 1977 A new density relation for pure and saline water. *Deep-Sea Res.* **24**, 831–848.

GEBHART, B. & MOLLENDORF, J. C. 1978 Buoyancy-induced flows in water under conditions in which density extrema may arise. *J. Fluid Mech.* **89**, 673–707.

JOHNSON, R. S. 1978 Transport from a melting vertical ice surface in saline water. M.S. thesis, State University of New York at Buffalo.

JOINT PANEL ON OCEANOGRAPHIC TABLES AND STANDARDS 1966 *International Oceanographic Tables.* Nat. Inst. Oceanog. G.B., Wormley, Godalming, Surrey.

JOSBERGER, E. G. & MARTIN, S. 1981 Laminar and turbulent boundary layers adjacent to melting vertical ice walls in salt water. *J. Fluid Mech.* **111**, 439–473.

LYMAN, J. & FLEMING, R. H. 1940 *J. Mar. Res.* **3**, 134–139.

WILSON, N. W. & VYAS, B. D. 1979 Velocity profiles near a vertical ice surface melting into fresh water. *Trans. A.S.M.E.* C., *J. Heat Transfer* **101**, 313–317.